# Supplementary Information for Designing Active Particles for Colloidal Microstructure Manipulation *via* Strain Field Alchemy

Bryan VanSaders[1], Sharon C. Glotzer[1,2,3]

[1]Department of Materials Science and Engineering, University of Michigan, Ann Arbor, Michigan 48109, United States

[2]Department of Chemical Engineering, University of Michigan, Ann Arbor, Michigan 48109, United States

[3]Biointerfaces Institute, University of Michigan, Ann Arbor, Michigan 48109, United States

June 25, 2019

## S1 Study Work-flow

This study utilizes several forms of simulation and characterization which feed into the final result. Figure S1 shows a schematic view of the flow of information and use of different simulation methods.

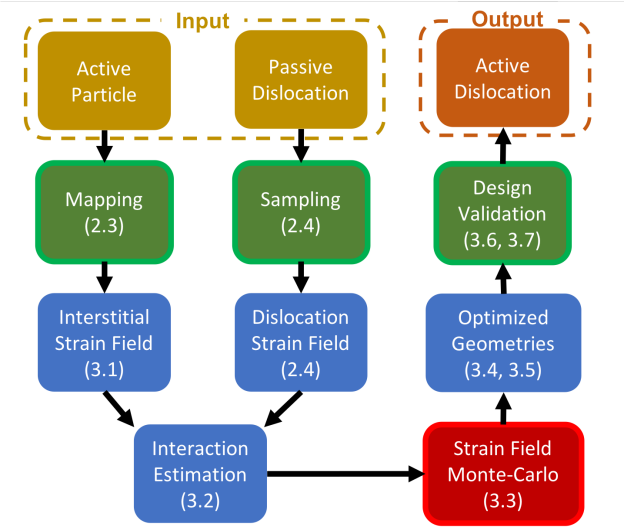


Figure S1: Schematic flow of information in this study. Green boxes indicate that molecular dynamics methods are used in that step. The red box indicates our newly developed strain alchemy algorithm. Boxes are labeled with matching sections when appropriate.

## S2 Dislocation Preparation

Line and loop dislocations used in this study were prepared for MD simulation by slicing of an initially perfect crystal domain. Fig. S2ai-ci shows the process for the preparation of arrays of line dislocations. Fig. S2aii-cii shows the same for loop dislocations.

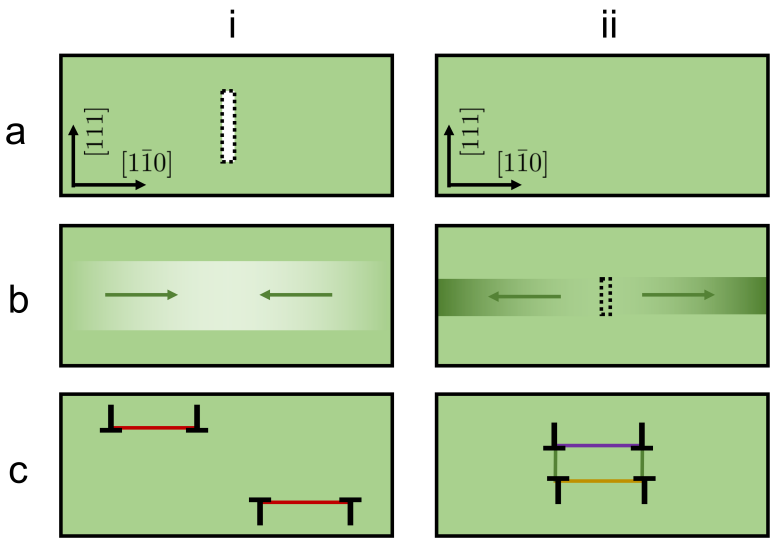


Figure S2: Schematic of how line dislocation arrays (column **i**) and dislocation loops (column **ii**) are prepared for MD simulation. **ai** An initially perfect crystal domain (green), has a rectangular section deleted from it (dashed box). The deleted volume is as wide as the box, half as tall as the box, and one Burgers vector in thickness. **bi** Regions of the crystal within the central half of the simulation box are stretched (linearly) so as to fill in the deleted section (indicated here by a color gradient). **ci** Once MD simulation has begun, the distorted crystal rapidly relaxes into a pair of partial dislocations (indicated by $\perp$), connected by stacking faults (red lines). **aii** An initially perfect crystal domain (green). **bii** Regions of the crystal bounded by the loop glide cylinder are compressed (linearly) so as to open up a space (dashed box) into which an additional plane of particles is added. **cii** Once MD simulation has begun, the distorted crystal rapidly relaxes into a dislocation loop (indicated by $\perp$), connected by Shockley partials (green), Hirth (purple), and stair-rod dislocations (purple).

## S3 Accuracy of Strain Field Predictions

Using the eigenstrain representation of the probe particle as well as the true strain field sampled from an MD simulation, the accuracy of the eigenstrain mapping was investigated. Fig. S3 shows the strain free energy density of the sampled and calculated strain fields ($E/V$) *vs.* segment diameter ($D_{seg}$) for the complete particle geometry to strain field mapping.

The analytically calculated eigenstrain solution free energy remains quadratic for all starting vales of $D_{seg}$. The sampled strain free energy curve diverges from the quadratic prediction for large segment diameters. The strains produced by large diameter segments are too large to be treated accurately by the linear elastic approximations central to the methods used here. For this reason we restrict ourselves to exploring segmented rod particles with diameters less than $0.20D$. This caps the maximum relative prediction error (show in Fig. S3 inset) at 50% (in practice, high-fitness geometries we found to have lower diameters).

## S4 Strain Alchemy MC Details

The initial eigenstrain value ($e_i$) was set to 0.05 for all probe segments (and an upper constraint of $e_i = 0.15$ was set). The optimization temperature, $kT_{\text{alch}}$ was logarithmically decreased from a starting value of $10^{-2}$ to $10^{-3}$ over $10^5$ iterations. These temperature values were chosen so that the average acceptance likelihood transitions from high to low at the approximate midpoint of the run. At each MC iteration a move was randomly selected. For optimization of line-dislocation probes, strain type moves were chosen with a 90% probability, with the remainder being evenly split between $x$ and $z$ positional moves. Moves in $y$ were not considered, as they would lie parallel with the dislocation line direction. For loop-dislocation probes, $x$, $y$, and $z$ moves are permitted. Strain moves were chosen with 91% probability with the remainder of moves evenly split among $x$,$y$, and $z$. Fig. S4 shows the flow of the MC loop when multiple move types are employed.

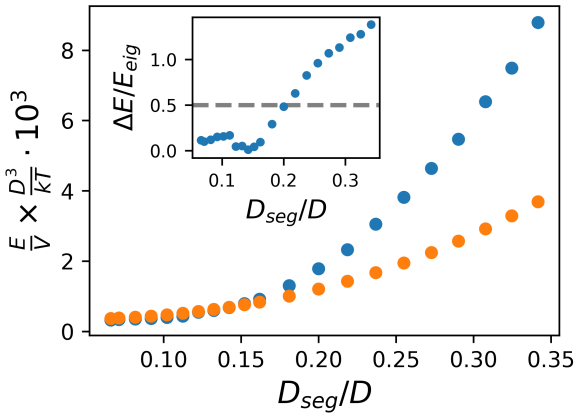


Figure S3: The strain free-energy density of a region around the probe interstitial versus segment diameter. The sampled values (in blue), diverge from the value predicted by the method of eigenstrains (in orange color) for segment diameters above $\sim 0.15D$. The inset shows relative error of the prediction, with a guide line at 50%. All curves have error bars (found *via* bootstrapping) that are smaller than the data markers.

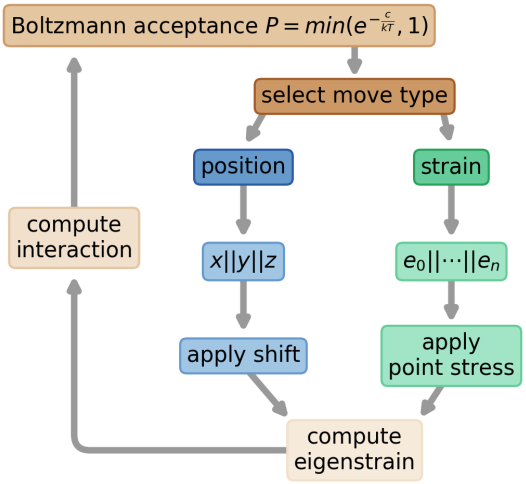


Figure S4: Schematic of the strain configuration MC loop with multiple move types, each having associated parameters from which to select. For positional moves, the Cartesian direction of movement $(x||y||z)$ is chosen. For strain moves a single-segment eigenstrain $(e_i)$ is chosen.